ELSEVIER

Clinical Neurophysiology 115 (2004) 1220–1232

www.elsevier.com/locate/clinph

Optimization of an independent component analysis approach for artifact identification and removal in magnetoencephalographic signals

Giulia Barbati[a,*], Camillo Porcaro[a], Filippo Zappasodi[b], Paolo Maria Rossini[a,c], Franca Tecchio[a,b]

[a]*Department of Neuroscience, AFaR – Center of Medical Statistics and Information Technology, Fatebenefratelli Hospital, Isola Tiberina, Lungotevere degli Anguillara 12, 00153 Rome, Italy*
[b]*ISTC Institute of Science and Technologies of Cognition, CNR, Rome, Italy*
[c]*Neurologia Clinica, Università Campus Biomedico, Rome, Italy*

Accepted 15 December 2003

Abstract

Objective: To propose a noise reduction procedure for magnetoencephalography (MEG) signals introducing an automatic detection system of artifactual components (ICs) separated by an independent component analysis (ICA) algorithm, and a control cycle on reconstructed cleaned data to recovery part of non-artifactual signals possibly lost by the blind mechanism.

Methods: The procedure consisted of three main steps: (1) ICA for blind source separation (BSS); (2) automatic detection method of artifactual components, based on statistical and spectral ICs characteristics; (3) control cycle on 'discrepancy,' i.e. on the difference between original data and those reconstructed using only ICs automatically retained. Simulated data were generated as representative mixtures of some common brain frequencies, a source of internal Gaussian noise, power line interference, and two real artifacts (electrocardiogram = ECG, electrooculogram = EOG), with the adjunction of a matrix of Gaussian external noise. Three real data samples were chosen as representative of spontaneous noisy MEG data.

Results: In simulated data the proposed set of markers selected three components corresponding to ECG, EOG and the Gaussian internal noise; in real-data examples, the automatic detection system showed a satisfactory performance in detecting artifactual ICs. 'Discrepancy' control cycle was redundant in simulated data, as expected, but it was a significant amelioration in two of the three real-data cases.

Conclusions: The proposed automatic detection approach represents a suitable strengthening and simplification of pre-processing data analyses. The proposed 'discrepancy' evaluation, after automatic pruning, seems to be a suitable way to render negligible the risk of loose non-artifactual activity when applying BSS methods to real data.

Significance: The present noise reduction procedure, including ICA separation phase, automatic artifactual ICs selection and 'discrepancy' control cycle, showed good performances both on simulated and real MEG data. Moreover, application to real signals suggests the procedure to be able to separate different cerebral activity sources, even if characterized by very similar frequency contents.

Keywords: Independent component analysis; Blind source separation; Automatic detection; Discrepancy

1. Introduction

When studying the cerebral activity through neurophysiological techniques, such as electroencephalography (EEG) and magnetoencephalography (MEG), the main goal is the discrimination of different sources of electrical activity. The first step in this direction is to separate the 'cerebral' sources from 'the others' generated by non-cerebral sources, these latter often of such intensities that the former ones are hidden (Zappasodi et al., 2001). Typically, a MEG sensor measures the mixture of original source signals with an adjunctive noise (Del Gratta et al., 2001). This mixture comes from both the 'wanted' sources and those 'to be discharged' (called artifacts).

Independent component analysis (ICA) is a promising approach that can be useful for the elimination of artifacts and noise from biomedical signals. Since the pioneering work of Scott Makeig and collaborators (Makeig et al., 1996) it is generally accepted that ICA is a good tool for

* Corresponding author. Tel.: +39-06-683-7300; fax: +39-06-683-7360.
E-mail address: giulia.barbati@afar.it (G. Barbati).

1388-2457/$30.00
doi:10.1016/j.clinph.2003.12.015

isolating artifacts in EEG and MEG data (Delorme and Makeig, in press; Vigario et al., 1997; Ziehe et al., 2000, 2001; Cao et al., 2000), but not much has still been achieved, except for the EEG recordings (Vorobyov and Cichocki, 2002; Delorme et al., 2001), about the criteria for selecting artifactual components in practical ICA applications. The aim of this study is to present an automatic detection procedure that can assist researchers in classifying the obtained independent components (ICs) as cerebral or non-cerebral (artifacts and noise) sources based on IC statistical properties (kurtosis, entropy) and spectral characteristics (Power Spectrum Density = PSD).

Moreover, the present method allows better signal reconstruction, i.e. the retro-projection of the automatically retained ICs: the difference between the original recorded data and the reconstructed ones is computed and called 'discrepancy.' Whenever a non-artifactual part of discrepancy is identified on the basis of its spectral characteristics, it is added to the reconstructed signal.

Section 2 describes the signal-generating model and each step of the proposed blind noise-reduction procedure; Section 2.1 makes some considerations about mathematical ICA assumptions in a MEG data context and presents the ICA algorithm used; Section 2.2 details the automatic detection method based on statistical and spectral component characteristics. Section 2.3 presents simulated and real data chosen to test the effectiveness and coherence of the proposed method. In Section 3 the results of each step of the procedure are provided. Finally, in Section 4, the significance of the results is discussed.

2. Model and procedure

We assume that the set of the observed MEG signals is generated by a mixing noisy model:

$$\mathbf{x}(t) = \mathbf{A}\mathbf{s}(t) + \mathbf{v}(t) \tag{1}$$

where $t = 0, 1, 2, ..., T$ is the discrete sampling time; $\mathbf{x}(t) = [x_1(t), ..., x_n(t)]^T$ is a n-dimensional vector of the observed noisy signal recorded by n sensors; $\mathbf{A}$ is a $n \times m$ unknown full-rank mixing matrix; $\mathbf{s}(t) = [s_1(t), ..., s_m(t)]^T$ is a m-dimensional unknown vector of primary sources ($n \geq m$); $\mathbf{v}(t)$ is a n-dimensional unknown vector of additive external spatially uncorrelated Gaussian noise that represents instrumental noise, as shown in Fig. 1a.

Furthermore, we assume that the vector $\mathbf{s}(t)$ contains a subset of useful or non-artifactual sources (brain activity) and artifactual sources (e.g. heartbeat, eye blinks, ocular movements, etc.) and that $\mathbf{s}(t)$ is not correlated with external noise; our objective is to reduce the influence of additive noise $\mathbf{v}(t)$ and to eliminate artifacts.

In other words, our task is to obtain corrected or 'cleaned' sensor signals which contain only 'interesting' (non-artifactual) sources. Sensor signals are processed by an ICA demixing system that is described by the following general model:

$$\mathbf{y}(t) = \mathbf{W}\mathbf{x}(t) \tag{2}$$

where $y(t) = [y_1(t), ..., y_m(t)]^T$ is an m-dimensional vector of the estimated ICs and $\mathbf{W}$ is a separation matrix, i.e. the estimate of the unknown mixing matrix $\mathbf{A}$:

$$\mathbf{W} = \hat{\mathbf{A}}^{+} \tag{3}$$

where the apex ' + ' denotes the inverse matrix. The outputs of the ICA demixing system pass through an automatic 'detection system' which takes the binary decision {0,1}, that is, to reject or to retain the corresponding IC.

Then, the retained ICs denoted as $\hat{\mathbf{y}}_\mathbf{k}$ ($k \leq m$) pass through the inverse system represented by the inverse $\mathbf{W}^{+}$ of the estimated separation matrix so to reconstruct data:

$$\mathbf{x}^{\mathbf{p}}_{\mathbf{Rec}} = \mathbf{W}^{+}_{\mathbf{k}}\hat{\mathbf{y}}_{\mathbf{k}} \tag{4}$$

where the apex $\mathbf{p}$ stresses that a part of the original signals could be not explained by the selected ICs and $\mathbf{W}^{+}_{\mathbf{k}}$ denotes the corresponding selected k columns of $\mathbf{W}^{+}$. We then define discrepancy as:

$$\mathbf{d} = \mathbf{x} - \mathbf{x}^{\mathbf{p}}_{\mathbf{Rec}} = \mathbf{x} - \mathbf{W}^{+}_{\mathbf{k}}\mathbf{W}_{\mathbf{k}}\mathbf{x} = [\mathbf{I} - \mathbf{W}^{+}_{\mathbf{k}}\mathbf{W}_{\mathbf{k}}]\mathbf{x} \tag{5}$$

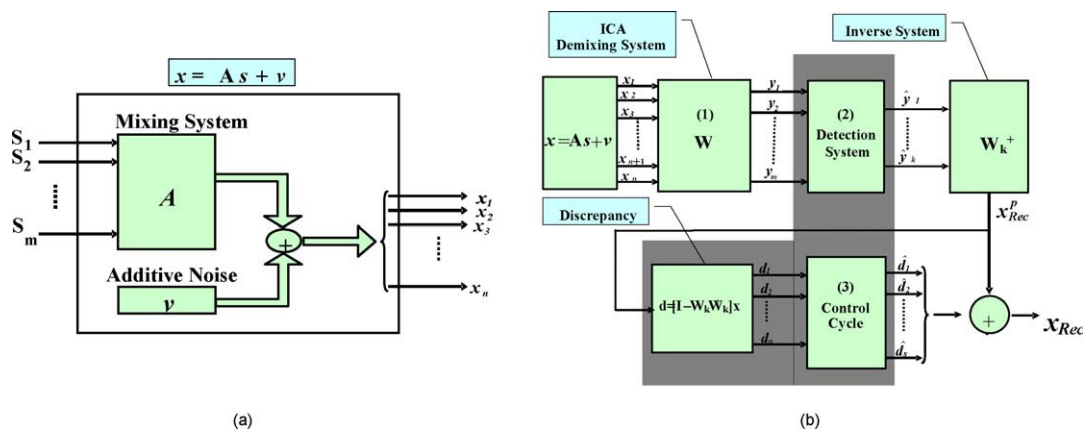

Fig. 1. (a) Block diagram of the mixing noisy model. (b) Block diagram illustrating the three main steps of the proposed blind noise-reduction procedure: (1) ICA demixing system; (2) detection system; (3) control cycle.

To verify and possibly improve the performance of the retro-projection process, we carry out a control cycle by examining the spectral characteristics of the n-dimensional discrepancy vector $\mathbf{d}(t) = [d_1(t), ..., d_n(t)]^T$ and by adding, when evaluated necessary, some 'useful' (non-artifactual) discrepancies $\hat{\mathbf{d}}_\mathbf{s}$ ($s \leq n$) to the output of the system (4):

$$\mathbf{x_{Rec}} = \mathbf{x^p_{Rec}} + \hat{\mathbf{d}}_\mathbf{s} \tag{6}$$

At the end of this process we obtain the final n-dimensional vector of the reconstructed sensor signals $\mathbf{x_{Rec}}(t) = [x_{\mathrm{Rec}_1}(t), ..., x_{\mathrm{Rec}_n}(t)]^T$ of the cleaned data, as shown in Fig. 1b.

In the noisy model (1) after separation (2) the estimated ICs contain both sources and additive noise:

$$\mathbf{y}(t) = \mathbf{W}\mathbf{x}(t) = \mathbf{W}(\mathbf{A}\mathbf{s}(t) + \mathbf{v}(t)) = \hat{\mathbf{s}}(t) + \mathbf{W}\mathbf{v}(t) \tag{7}$$

This implies that if one IC is to be rejected, two types of noises are rejected in one go. Otherwise, it can happens sometimes that a filtering procedure should be performed for the non-artifactual ICs (i.e. not automatically removed) in order to reduce the term **Wv(t)**. In our work the filter used is a Butterworth bandpass filter (forward-backward) of order **z = 2** and bandwidth = **[a,b]** depending on the cases; the same filtering procedure is applied on selected discrepancies, that are in the same scale of the original recorded signals.

2.1. ICA algorithm

The use of ICA algorithm is based on three assumptions: (1) the existence of sources that are statistically independent from one another; (2) the instantaneous and linear mixing of their contributions to the sensors; (3) the stationarity of the mixing process. A detailed discussion of all ICA assumptions and requirements can be found in many publications regarding the mathematics of ICA (Te-Won Lee, 1998; Hyvärinen et al., 2001; Cichocki and Amari, 2002). Briefly, these hypotheses in a MEG data context can be clarified by the following considerations: independence refers solely to the statistical relationships among the amplitude distributions of the signals involved; it can be reasonably assumed that the mixing process be instantaneous since MEG activity is somewhat below 1 kHz and the quasi-static approximation of the Maxwell equations holds (Del Gratta et al., 2001); the stationarity of the mixing process is compatible with the widely accepted description of brain sources as current dipoles and, within this model, it corresponds to the existence of sources with fixed locations and orientations but time-varying amplitudes.

Concerning the noisy model (1), recently several robust-to-external-noise algorithms have been proposed (Choi and Cichocki, 2000; Hyvärinen, 1999); among the large number of algorithms available, we used a version of the cumulant-based algorithm named 'Cumulant-based Iterative Inversion' (CII) proposed by Cruces and collaborators (Cruces-Alvarez et al., 2000, 2002) and implemented in the package ICALAB of Cichocki and Amari under the name 'ERICA' (Equivariant Robust ICA – based on cumulants). We will not explain here the details of the algorithm (see Appendix B): as shown by the authors, the key point is that this algorithm is 'robust' in the sense that, for signals contaminated by an additive external Gaussian noise, the obtained estimate are asymptotically unbiased; since in practice the cumulants should be estimated from a finite data set, the robustness property holds when there is a sufficient number of samples (typically ≥ 5000) which enables reliable estimates of the cumulants.

In our version of the algorithm, that we call 'Cumulant-based Iterative Inversion in Signal Subspace' (CIISS), we achieve a 'robust reduction' of the problem dimensionality by using a robust pre-whitening phase based on the signal subspace (SS) criterion (Cichocki and Amari, 2002), before starting with the CII separation phase. In fact, usually ICA algorithms include a first phase of data 'whitening,' that conveniently transforms the original signals into a new set of signals having zero mean and unit variance and operating, if necessary, also a dimensionality reduction (Hyvärinen et al., 2001; Ikeda and Toyama, 2000; Belouchrani and Cichocki, 2000). Generally, this is done by applying the principal component analysis (PCA) technique, so determining a threshold on the eigenvalue decreasing sequence obtained from the data covariance matrix that separates signals from noise, i.e. it is assumed that the first m of the n eigenvalues forms an m-dimensional signal subspace, whereas the remaining $n - m$ eigenvalues and the corresponding eigenvectors define a $(n - m)$-dimensional noise subspace. In the present CIISS algorithm, this whitening and reduction phase is performed by subtracting an estimate of the noise variance to the signal subspace (see Appendix A).

2.2. Detection and classification of ICs

Four markers were considered for artifact recognition: percentage of kurtosis-outlier segments ($\mathrm{Kurtosis_o}$), global kurtosis coefficient ($\mathrm{Kurtosis_g}$), percentage of entropy-outlier segments ($\mathrm{Entropy_o}$) – all based on IC statistical properties – and correlation coefficient with PSD of typical artifacts (PSD corr), based on IC spectral characteristics.

2.2.1. IC marker using $Kurtosis_o$

In the segment-partition approach we computed the measure of the kurtosis of the jth segment of the ith IC as:

$$K^i(j) = {}^{i,j}m_4 - 3^*({}^{i,j}m_2^2) \tag{8}$$

where ${}^{i,j}m_n = E\{({}^{i,j}x - {}^{i,j}m_1)^n\}$ is the nth central moment of all the activity values of the jth segment of the ith IC, ${}^{i,j}m_1$ the mean, and E the expectancy function (the average); we used the built-in *kurt.m* function of MATLAB 6.1 (throughout this study all computations are made using MATLAB version 6.1).

Kurtosis is positive for 'peaked' activity distributions, typical of artifacts such as ECG and EOG; on the other hand, kurtosis is negative for 'flat' activity distributions; as pointed out in Delorme et al. (2001) we can think that this kind of activity is typical of noise. Therefore, since we look for artifactual ICs, or in other words for 'outlier' components, these measure distributions have been normalized with respect to all ICs to 0-mean and 1-standard deviation: in this way, thresholds in terms of number of standard deviations from the mean were applied (classical thresholds set at ± 1.64) and, if a certain percentage of segments (in our applications more than 20%) exceeded rejection thresholds, the corresponding IC was marked for rejection.

2.2.2. IC marker using $Kurtosis_g$

The global kurtosis coefficient of the *i*th IC was computed as:

$$K^i = {}^i m_4 - 3^*({}^i m_2^2) \tag{9}$$

where, as above, ${}^i m_n = E\{({}^i x - {}^i m_1)^n\}$ is the *n*th central moment of all the activity values of the *i*th IC, the mean, and *E* the expectancy function (the average). Using eq. (9), kurtosis is zero for Gaussian distributions; since in the previous threshold approach only severely super- and sub-Gaussian ICs were identified, the IC showing the minimum positive $Kurtosis_g$ value was marked in order to recognize Gaussian noise components. Also here we used the built-in *kurt.m* function of MATLAB 6.1.

2.2.3. IC marker using $Entropy_o$

An approximate measure of entropy of the *j*th segment of the *i*th IC is defined as:

$$H^i(j) = -\sum_{x \in j} p_j^i(x) \log\left(p_j^i(x)\right) \tag{10}$$

where $p_j^i(x)$ is the probability of observing the activity values x in the distribution of activity in the *j*th segment from the *i*th IC. Only the threshold procedure was used in this case: we preferred to approximate probability densities during short intervals rather than throughout the recording length so to simplify both computational task and interpretation of results. The more 'random,' i.e. unpredictable and unstructured, a component is, the larger its entropy is; therefore we can think that larger segment-entropy values can help us to detect uninteresting ICs; on the other hand, if segment-entropy values are quite below the mean, this indicates that the random variable is contained in some limited intervals with high probabilities, just as happens in certain types of artifacts with 'spiky' probability densities.

The distributions of the segment-entropy measures were normalized to 0-mean and 1-standard deviation with respect to all ICs; even this time, we used standard thresholds set at ± 1.64 and, if a significant percentage (set at 20%) of segments exceeded rejection thresholds, the corresponding IC was marked for rejection. To compute entropy values, we wrote a MATLAB routine; basically, we approximated ICs-segments probability density functions (pdfs) computing frequency tables of data rounded off to the second decimal and then we computed entropy as reported in eq. (10).

2.2.4. IC Marker using PSD corr

The PSDs of a real electrocardiogram (ECG) and a real electrooculogram (EOG) were calculated. Then, the correlation coefficients between the PSD of the estimated ICs and the PSD of ECG and EOG were computed; for each artifact, the ICs showing the maximum correlation coefficient values were marked for rejection (PSD corr). Naturally, this procedure can be improved by using, when available, data from the same subject-electrical reference channels (ECG, EOG), recorded simultaneously with the MEG/EEG.

For each IC, the automatic detection system took the reject decision when at least one of the criteria based on $Kurtosis_o$, $Kurtosis_g$, $Entropy_o$ and PSD corr was satisfied.

As reported at the opening of Section 2, some selected components (i.e. not automatically removed) were suitably filtered if necessary, and in this case indicated as IC*.

2.3. Test data description

2.3.1. Simulated data

As shown in Fig. 2a, we generated three sources, S1, S2 and S3, at frequencies of 10, 20 and 30 Hz, respectively (with a frequency-band amplitude of 2 Hz); a source S4 of Gaussian internal noise, a source S5 representing typical line interference at 50 Hz, and two artifactual sources, that is, S6, from a real ECG, and S7, from a real EOG. These source signals were linearly mixed through a randomly generated mixing matrix A ($T = 5000$ points at a sampling frequency of 1000 Hz). Following the noisy model (1), we added a matrix of Gaussian external noise to the mixed signals. In Fig. 2b, 6 out of 28 mixed noisy signals we obtained are shown.

2.3.2. Real MEG data

The MEG data were recorded in three healthy volunteers (PIRO 36 years old, male; RIFI 24 years old, female; BRCH 74 years old, female) after the Standard Ethical Procedures according to the Declaration of Helsinki. Subjects were comfortably lying with open eyes and spontaneous activity was recorded (0.048–250 Hz bandpass, sampling rate 1000 Hz) from hemispheric rolandic region by positioning a single sensor centered around C3 or C4 site of the International 10–20 electroencephalographic system (C3 for RIFI and BRCH, C4 for PIRO). Signals were detected by 28 channels (16 internal axial gradiometers and 12 peripheral magnetometers) regularly distributed on a spherical surface covering an area of about 180 cm^2 (Tecchio et al., 1997; Zappasodi et al., 2001). The noise spectral density of each sensor channel was 5–7 fT/Hz at 1 Hz. In one subject, pairs of Ag-AgCl cup electrodes were placed medially just above and below the right eye for

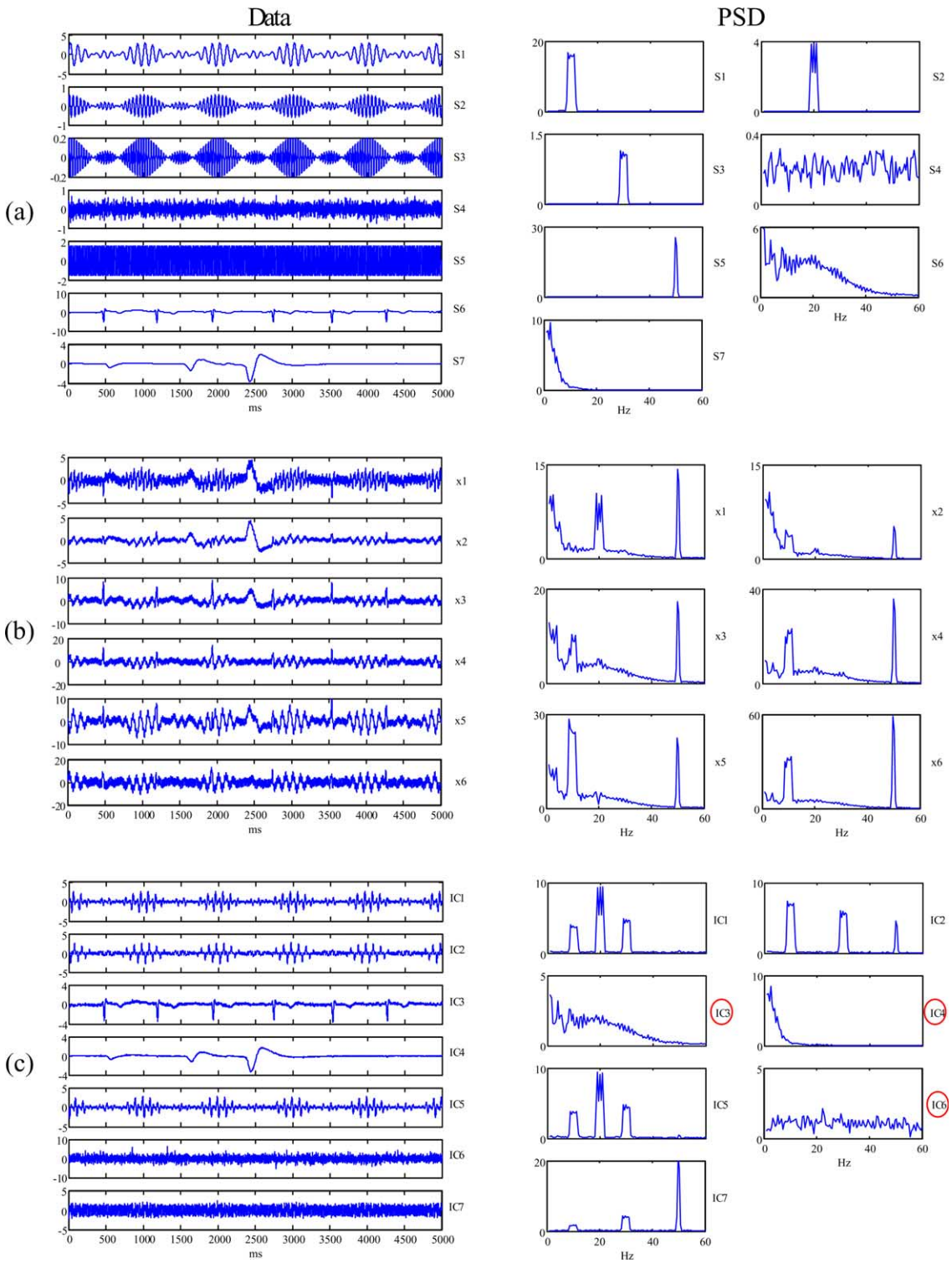

Fig. 2. Simulated Data. (a) Simulated sources S1 at 10 Hz, S2 at 20 Hz, S3 at 30 Hz, S4 Gaussian noise, S5 at 50 Hz, S6 from a real ECG and S7 from a real EOG and their PSD (right). (b) Sample of mixed noisy signals and their PSD. (c) Estimated ICs and their PSD: IC1, IC2, IC5, and IC7 correspond to activities at 10, 20, 30 and 50 Hz; IC3 and IC4 correspond to ECG and EOG, respectively; IC6 captured residual Gaussian noise. Circles indicate ICs automatically rejected.

the electrooculographic activity recordings and the electrocardiogram was recorded through a bipolar standard montage for polygraphy with one thoracic derivation (filtering and sampling parameters as for MEG).

These three data samples were chosen as representative of, respectively: PIRO, short noisy data; RIFI, longer tract affected mostly by EOG artifact; BRCH, longer tract affected mostly by ECG artifact.

3. Results

3.1. Simulated data

We applied ICA to the data generated as described above. The estimated ICs with the corresponding PSD are shown in Fig. 2c.

We applied the detection system by computing a 7-segments partition of the estimated ICs and results are shown in Fig. 3 and summarized in the section 'Simulated data' of Table 1. Kurtosis$_o$ detected IC3 (Fig. 3a), Entropy$_o$ detected IC4 (Fig. 3b), PSD corr marked IC3 and IC4 (Fig. 3c) with ECG and EOG, respectively, and finally Kurtosis$_g$ detected IC6 (Fig. 3d).

Therefore IC3, IC4 and IC6 were rejected on the basis of the automatic detection system; by means of a visual PSD inspection of the ICs, we can observe (Fig. 2c) that IC1, IC2, IC5 and IC7 isolated brain activity sources at 10, 20 and 30 Hz, even if IC2 and especially IC7 were still corrupted by interference at 50 Hz; IC3 and IC4 identified ECG and EOG, respectively, and IC6 corresponded to Gaussian noise.

The control cycle on discrepancy confirmed the good performance of the retro-projection process using retained IC1, IC2*, IC5 and IC7*, since discrepancy contained only artifacts and noise. We filtered out 50 Hz from IC2 and IC7 using a Butterworth bandpass filter of **z = 2** and bandwidth = **[48,52].**

3.2. Real MEG data

In the first real-data example, we applied ICA to a PIRO subset of MEG recordings (10 000 points, 10 s); a sample of the original data and their PSD are shown in Fig. 4a. From the PSD of the original data, the presence of low-frequency activity (<5 Hz) corresponding to ocular and cardiac artifacts was clearly visible (see for comparison the PSD shown in Fig. 2a, sources S7 and S6); we used only a portion of the original recording since we aimed to explore blind source separation performance in a small data-dimension context. The estimated ICs and their PSD are shown in Fig. 4b.

We applied the detection system by computing a 14-segments partition of the estimated ICs and results are summarized in the section 'PIRO' of Table 1. Kurtosis$_o$ did not detect any component, Entropy$_o$ detected IC10, PSD corr marked IC6 for both ECG and EOG, and finally Kurtosis$_g$ detected IC8. This means that 3 ICs (IC6, IC8

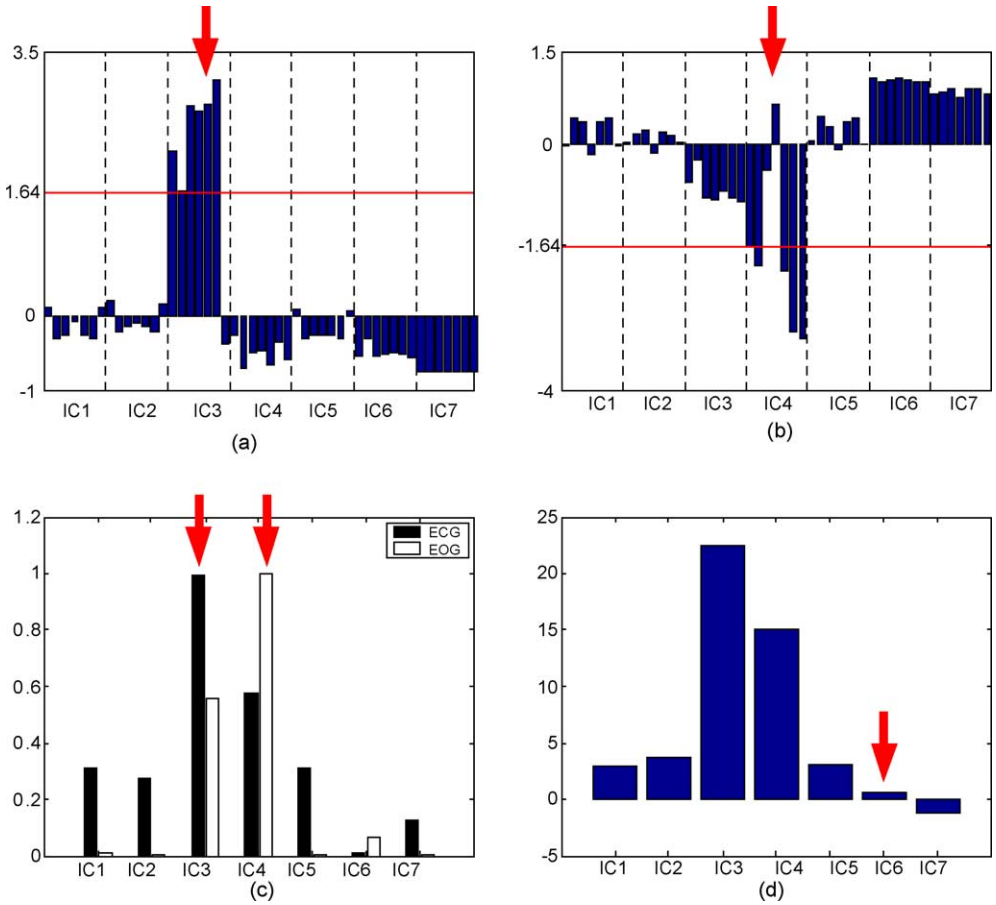

Fig. 3. Automatic detection system on estimated ICs from simulated data; arrows indicate ICs marked for rejection. (a) Kurtosis$_o$ marked IC3, corresponding to ECG, for rejection; (b) Entropy$_o$ marked IC4, corresponding to EOG; (c) PSD corr marked IC3 for ECG and IC4 for EOG; (d) Kurtosis$_g$ marked IC6.

Table 1
MEG data

		$Kurtosis_o$ (%)	$Entropy_o$ (%)	PSD corr		$Kurtosis_g$
				ECG	EOG	
Simulated data	IC1	0	0	0.3112	0.0080	3.0417
	IC2*	0	0	0.2738	0.0037	3.7717
	IC3	**86**	0	**0.9957**	0.5542	22.406
	IC4	0	**71**	0.5779	**0.9999**	15.042
	IC5	0	0	0.3113	0.0076	3.0475
	IC6	0	0	0.0077	0.0681	**0.5895**
	IC7*	0	0	0.1275	0.0073	−1.1834
PIRO	IC1*	0	0	0.7111	0.3748	−0.2801
	IC2*	7	0	0.7846	0.4950	1.0600
	IC3	0	7	0.5867	0.2990	0.6476
	IC4*	7	0	0.6484	0.4501	0.7178
	IC5	14	7	0.6232	0.2336	1.6167
	IC6	14	14	**0.8345**	**0.7184**	2.5784
	IC7*	0	14	0.7593	0.5422	2.2827
	IC8	7	0	0.8000	0.4292	**0.4474**
	IC9*	0	0	0.7926	0.4901	−0.3109
	IC10	7	**57**	0.6733	0.3480	4.5413
	IC11*	7	0	0.5619	0.5017	−0.4297
RIFI	**IC1**	**64**	0	0.6355	**0.9375**	2.9073
	IC2	0	**100**	0.8071	0.4310	0.0483
	IC3*	3	0	0.6688	0.7067	0.4286
	IC4	5	**39**	0.6868	0.7024	1.5164
	IC5	0	0	0.7073	0.7201	0.1937
	IC6	0	0	0.7999	0.6433	0.5230
	IC7	0	0	**0.8483**	0.7187	0.2448
	IC8	0	0	0.5818	0.3485	0.8696
	IC9	0	0	0.7969	0.4165	**0.0393**
	IC10	5	0	0.7774	0.6970	0.9881
BRCH	**IC1**	5	0	0.6474	**0.7238**	0.9390
	IC2	0	0	0.6949	0.2067	0.2374
	IC3*	11	0	0.8513	0.6651	2.3184
	IC4	0	0	0.5420	0.1210	0.3322
	IC5	0	**100**	0.7511	0.3009	0.0675
	IC6	**28**	0	**0.8730**	0.6908	1.5013
	IC7	3	0	0.7978	0.3168	0.3778
	IC8	0	0	0.7496	0.3063	**0.0379**
	IC9	3	0	0.7006	0.2320	0.3358
	IC10	3	0	0.8346	0.3730	0.3748

Marker values in simulated and real cases. $Kurtosis_o$ and $Entropy_o$ are percentages of outlier segments; PSD corr is the correlation coefficient value, with respectively ECG and EOG spectra; $Kurtosis_g$ is the global kurtosis coefficient value. In bold are detected ICs and corresponding marker values; asterisks indicate filtered ICs.

and IC10) were automatically detected by means of the proposed switching system. Using visual inspection of components PSD and time activations as shown in Fig. 4b, we could have rejected IC6, IC8, IC9 and IC10.

We then reconstructed the data with the elimination of just the ICs automatically rejected by the system. A sample of the PSD of the reconstructed data with retained ICs is shown in Fig. 4c; the control cycle on discrepancy showed that a peak at the 10 Hz activity was not captured by the initial reconstructed data. Therefore, non-artifactual detected filtered discrepancy channels were added in order to obtain the final reconstructed data, as shown in Fig. 4d. In the discrepancy vector we selected 9 out of 28 channels, filtered using a Butterworth bandpass filter of **z = 2** and bandwidth **= [5,50]**; moreover, we filtered IC1, IC2, IC4, IC7, IC9 and IC11 with a Butterworth bandpass filter of**z = 2** and bandwidth = **[5,50]**.

In the second real-data example, we applied ICA to 3 min (180 000 points) of RIFI MEG recordings; a sample of the original data and their PSD are shown in Fig. 5a. Also here, low frequencies clearly over-represented in a healthy subject were visible (compare with Fig. 2a, source S7); the estimated ICs and their PSD are shown in Fig. 5b.

We applied the detection system by computing a 36-segments partition of the estimated ICs. Results are summarized in the section 'RIFI' of Table 1. $Kurtosis_o$ detected IC1, $Entropy_o$ detected IC2 and IC4, PSD corr marked IC1 and IC7 for EOG and ECG, respectively, and finally $Kurtosis_g$ detected IC9. This means that 5 ICs were automatically detected by means of the proposed switching system. Adopting visual criteria we could have rejected: IC1, IC2, IC4, IC6, IC7 and IC9.

We reconstructed data with the elimination of just the ICs automatically rejected by the system. A sample of the PSD of the reconstructed data with retained ICs is shown in Fig. 5c. We filtered IC3 using a Butterworth bandpass filter of **z = 2** and bandwidth = **[5,50]**.

The control cycle on discrepancy confirmed the good performance of the retro-projection process, since discrepancy contained only artifacts and noise.

In the third real-data example, we applied ICA to 3 min of BRCH MEG recordings; some channels of the original data and their PSD are shown in Fig. 6a. From both raw signals and their PSD we can recognize the presence of the cardiac artifact in a broad spectrum of frequencies ranging from 5 to 40 Hz (compare with Fig. 2a, source S6); furthermore, an over-representation of low frequencies probably due to ocular movements was present. The estimated ICs and their PSD are shown in Fig. 6b.

We applied the detection system by computing a 36-segment partition of the estimated ICs. Results are shown and summarized in the section 'BRCH' of Table 1. $Kurtosis_o$ detected IC6, $Entropy_o$ detected IC5, PSD corr marked IC1 and IC6 for ECG and EOG, respectively, and finally $Kurtosis_g$ detected IC8. Therefore, 4 ICs were automatically detected by means of the proposed switching system. We could have visually rejected 5 ICs: IC1, IC3, IC5, IC6 and IC8.

We reconstructed the data with the elimination of the ICs automatically rejected by the system; a sample of the PSD of the reconstructed data, with the selected ICs, is shown in Fig. 6c. The control cycle on discrepancy showed that a activity spectral peak at 10-Hertz was not captured by the initial reconstructed data; therefore, useful discrepancy filtered channels were added so to obtain the final reconstructed data, as shown in Fig. 6d. In the discrepancy vector we selected 12 out of 28 channels, filtered using

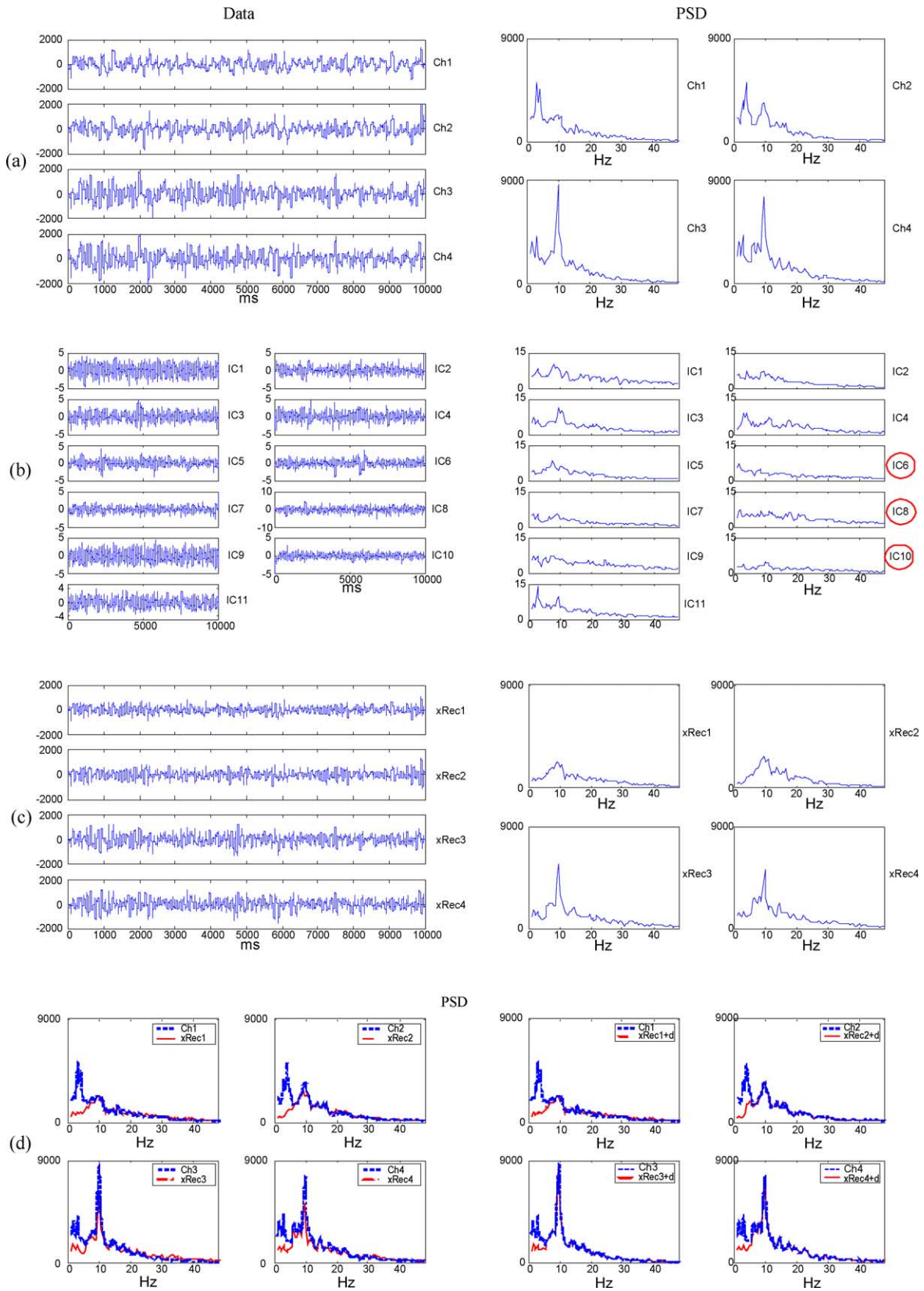

Fig. 4. PIRO real data. (a) Selection of 4 representative original PIRO signals and their PSD: is clearly visible the presence of low-frequency activity (< 5 Hz), corresponding to ocular and cardiac artifacts. (b) Estimated ICs (circles indicate automatically rejected components) and their PSD: IC6 was marked for rejection by PSD corr with both ECG and EOG; IC8 by Kurtosis_g and IC10 by Entropy_o. (c) The reconstructed data and their PSD. (d) Overlap between the 4 channels before (dotted line) and after (solid line) the data reconstruction, without (left) and with (right) adding 'non-artifactual' discrepancy.

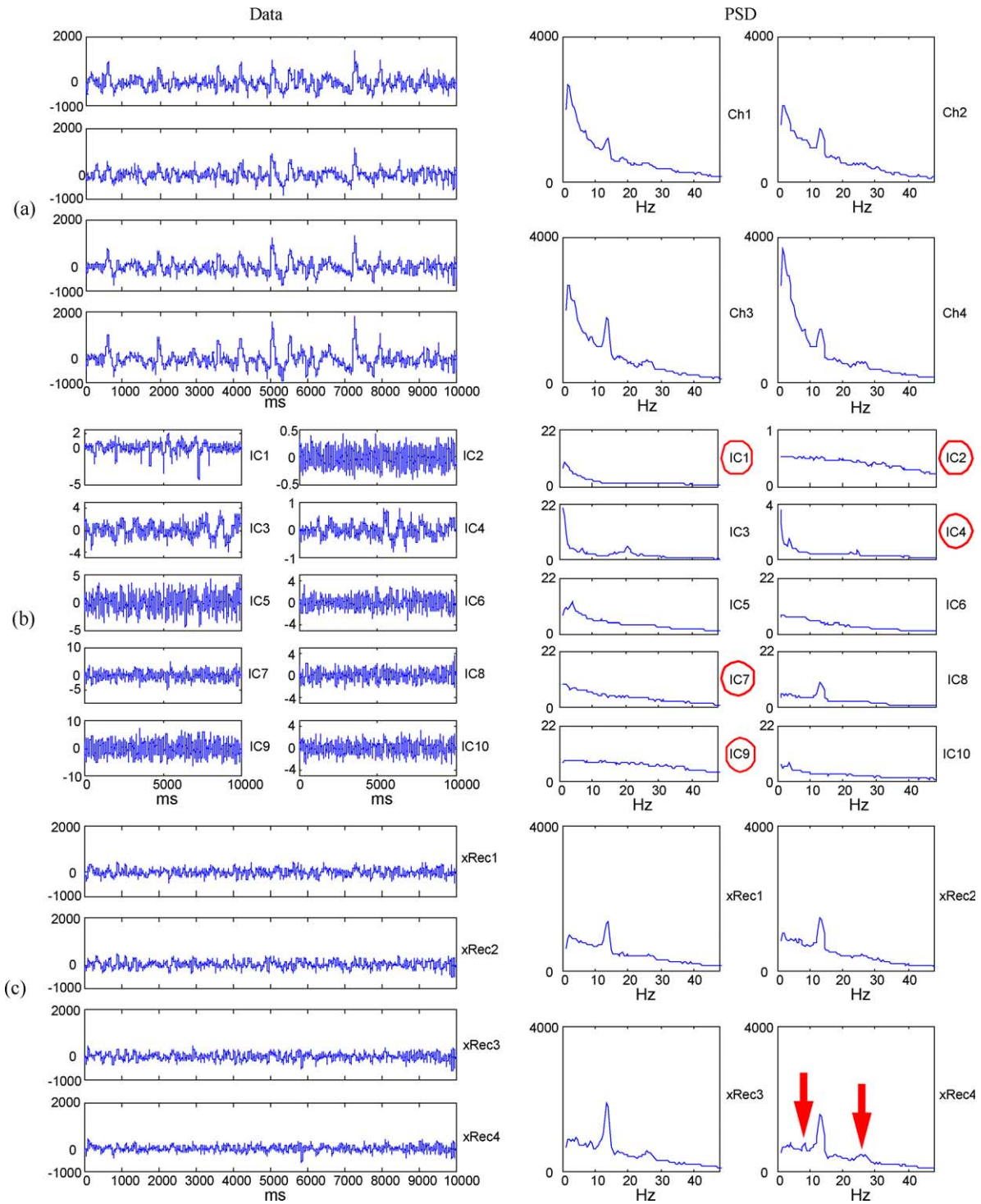

Fig. 5. RIFI real data. (a) Selection of 4 original RIFI signals and their PSD: are visible low frequencies clearly over-represented in a healthy young subject. (b) Estimated ICs and their PSD (PSD of IC2 and IC4 are on different scales): IC1 was marked by $Kurtosis_o$ and PSD corr with EOG, IC2 and IC4 by $Entropy_o$, IC7 by PSD corr with ECG, IC9 by $Kurtosis_g$ and were automatically rejected (circles). (c) The 4 reconstructed data signals and their PSD: arrows indicate 'interesting' (non-artifactual) frequency activities around 8 and 25 Hz, more evident after the successful discharge of confounding artifact activities (see Ch4 panel a right).

a Butterworth bandpass filter of **z = 2** and bandwidth = **[5,15]**; moreover, we filtered IC3 using a Butterworth bandpass filter of **z = 2** and bandwidth = **[5,50]**.

4. Discussion

In this work we proposed a method for blind artifact and noise identification and reduction in MEG signals, by using

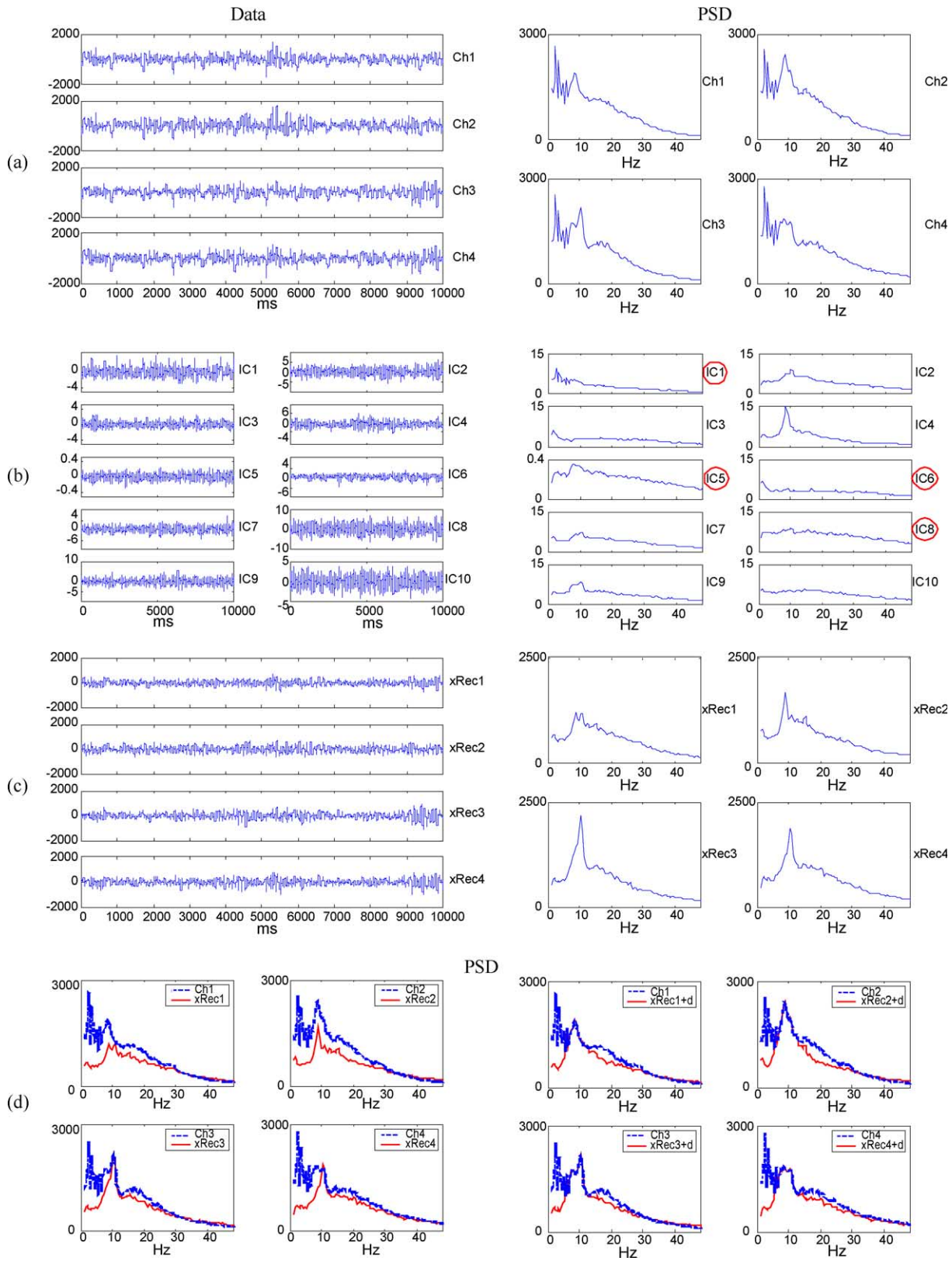

Fig. 6. BRCH real data. (a) Selection of 4 original signals and their PSD: from both raw-signal activations in time and their PSD it could be recognized the presence of the cardiac artifact in a broad spectrum of frequencies between 5 and 40 Hz and an over-representation of low frequencies. (b) Estimated ICs and their PSD (PSD of IC5 is on a different scale); IC1 was marked by PSD corr for ECG, IC5 by Entropy_o, IC6 by Kurtosis_o and PSD corr for EOG, IC8 by Kurtosis_g. (c) The 4 reconstructed data and their PSD. (d) Overlap between the 4 channels before (dotted line) and after (solid line) the data reconstruction, without (left) and with (right) adding non-artifactual discrepancy.

a procedure comprising three main steps: (1) ICA, (2) discrimination between cerebral (non-artifactual)/non-cerebral (artifactual) ICs by an automatic detection system, and (3) possible identification and addition of 'useful' discrepancies.

ICA demonstrates a powerful alternative for artifact cancellation with respect to classical segment-rejection approach, the latter being based on discarding segments of raw data that are hidden at a visual inspection because of the presence of artifacts. Moreover, ICA is mostly relevant when studying spontaneous activity, where no event-related average could be used for signal-to-noise ratio improvement, and allows suitable information extraction from shorter signal recordings.

The introduction of an automatic detection approach, by which a set of measures can isolate a significant number of artifactual ICs, results in a great simplification of successive data analyses. In particular, this data-driven detection system could be very useful for multichannel systems with hundreds of sensors, where a high number of ICs is produced and must be processed. The automatic selection was based not only on IC statistical properties such as those at the base of the algorithm estimation method, but also on IC spectral characteristics. It is to be noted that the PSD corr identified some ICs not marked by kurtosis and entropy criteria; this indicates that estimated ICs could have 'prototypical' spectral characteristics (for example, typical of electrocardiographic and electrooculographic artifactual signals) and suggests that including frequency information directly in the source-separation phase jointly with higher-order criteria could improve algorithm performance in specific MEG/EEG applications (Gorodnitsky and Belouchrani, 2001). In the simulated data context, the automatic markers diagnostic selection is optimal. In the real-data examples, the proposed automatic detection system agreed with a visual inspection in the 79% of cases on average. We based the retro-projection process on automatically retained ICs instead of on visually detected ones: besides the former procedure being obviously less time-consuming, we think that the latter could be seriously affected by the roughness of the cerebral activity spectra model that can be constructed by the researcher's experience, due for example to the high variability in PSD shapes among different subjects, and by the level of researcher attention. Certainly, there is a certain number of user-defined settings in the detection system parameters (length of segments, significant percentage of outlier-segments, level of thresholds) and further improvements could be made through the study of the robustness of the final rejection decision with respect to these parameters or through the research on possible other detection criteria. The scalp distribution of retro-projected ICs is generally used in literature in order to help the identification of artifactual components (Jung et al., 2000). Our procedure did not include this criterion; this feature could be suitable when studying patients affected by cerebral lesions, in whom low-frequency pathological activities could spatially overlap artifactual ones.

Since, to our knowledge, a numerical index to compare original and reconstructed data in BSS real applications is lacking, the difference between original and reconstructed data in the sensors space was considered. It has been proposed the possible addition of selected 'discrepancy' channels, with spectral characteristics of non-artifactual activity, to obtain final reconstructed data. In our opinion, this could be especially relevant when dealing with small-size data; in any case, we think it really is a crucial control cycle in reconstructing data through blind separation techniques. In the simulated data context the control cycle on discrepancy is redundant, but, on the contrary, it means a significant amelioration in two of the three real-data examples (i.e. PIRO and BRCH).

With respect to the artifact reduction in real applications, in the RIFI data example it can be noted that, in cleaned reconstructed signals, 'interesting' frequency activities around 8 and 25 Hz could be recognized (see Fig. 5c), after successfully discharge of confounding artifact activities. For instance, cerebral and artifactual activities could always coexist in the same frequency ranges: on one hand, in the RIFI example, the 8 Hz activity was masked by the artifactual one; on the other hand, in BRCH (see Fig. 6d), part of the potentially physiological 20 Hz activity was removed as an ECG artifact.

In the BRCH data case, it could be observed that different ICs (IC4 and IC2, IC7, IC9) described activities around 10 Hz with different frequency peaks. IC4 showed a clear maximum at 8.5 Hz whereas IC2, IC7 and IC9 at 10.0 Hz. It is known that the spontaneous activity generated in occipital areas and responding to visual stimuli (alpha rhythm), and the activity generated in the rolandic areas and responding to movement and somatosensory stimulation (mu rhythm) both fall in this range of frequencies. The latter is generally at slightly higher frequency than the former ($\sim$1 Hz), when compared in the same subject (Gastaut, 1952; Hari and Salmelin, 1997; Okada and Salenius, 1998). This finding suggests that ICA can be a powerful method for separating different 10 Hz cerebral sources, taking into account that a selection by simply bandpass filtering in such narrow bands will cause signal distortion. It is noteworthy that in simulated data, sources at 10, 20 and 30 Hz appeared together in more than one IC (see Fig. 2c: IC1, IC2, IC5 and IC7) while ECG and EOG were completely separated in two distinct ICs (ECG in IC3, EOG in IC4). This fact, together with the randomly-generated source mixing matrix, stresses that not the 'spatial' source distribution – lost in the random mixing process – but solely the different source statistical properties determined the estimated components. In fact, simulated sources at 10, 20 and 30 Hz are characterized by very similar distributions, which are definitely different from those of ECG and EOG, and these last two differ considerably from each other.

Therefore, the fact that in BRCH very similar frequencies appeared separated in different ICs suggests that the underlying neural activity could be separated on the basis of different generating mechanisms, although within very narrow frequency ranges and independently from spatial distribution.

In conclusion, the present noise reduction procedure, including ICA separation phase, automatic artifactual ICs selection and 'discrepancy' control cycle, showed good performances both on simulated and real MEG data. Moreover, application to real signals suggests the procedure to be able to separate different cerebral activity sources, even if characterized by very similar frequency contents.

Acknowledgements

The authors thank Professor Sergio A. Cruces-Álvarez and Dr Sergiy Vorobyov for kindly providing the CII algorithm.

Appendix A. Robust pre-whitening based on Signal Subspace criterion

We started the ICA algorithm by whitening and reducing the noisy data.

Whitening can in general be obtained by singular value decomposition (svd) of the data covariance matrix $\mathbf{R_{xx}} = \mathbf{E}\{\mathbf{x}\mathbf{x}^{\mathbf{T}}\}$:

$$svd(\mathbf{R_{xx}}) \rightarrow \tilde{\mathbf{x}} = \mathbf{\Lambda}^{-1/2}\mathbf{V}^{\mathbf{T}}\mathbf{x} = \mathbf{Q}\mathbf{x} \tag{A1}$$

where $\mathbf{V}$ contains the eigenvectors associated with the eigenvalues of $\mathbf{\Lambda} = diag\{\lambda_1 \geq \lambda_2 \geq ... \geq \lambda_n\}$ in descending order; in this way, we obtain a whitening matrix $\mathbf{Q}$ such that $\mathbf{R}_{\tilde{x}\tilde{x}} = \mathbf{I}_n$, the whitened data are zero-mean, unit variance and uncorrelated.

We achieve a 'robust reduction' of the dimensionality of the problem by using the signal subspace criterion, i.e. by assuming that the first m of the n eigenvalues forms an m-dimensional signal subspace, whereas the remaining n-m define a (n-m)-dimensional noise subspace. Consequently we can write:

$$\mathbf{R_{xx}} = \mathbf{V_x}\mathbf{\Lambda_x}\mathbf{V_x^T} = [\mathbf{V_S}, \mathbf{V_N}]\begin{bmatrix} \mathbf{\Lambda_S} & \mathbf{0} \\ 0 & \mathbf{\Lambda_N} \end{bmatrix}[\mathbf{V_S}, \mathbf{V_N}]^{\mathbf{T}}$$

$$= \mathbf{V_S}\mathbf{\Lambda_S}\mathbf{V_S^T} + \mathbf{V_N}\mathbf{\Lambda_N}\mathbf{V_N^T} \tag{A2}$$

where $\mathbf{V_S}$ contains the eigenvectors associated with the eigenvalues of $\mathbf{\Lambda_S} = diag\{\lambda_1 \geq \lambda_2 \geq ... \geq \lambda_m\}$ of the signal subspace, whereas $\mathbf{V_N}$ contains the eigenvectors associated with the eigenvalues of $\mathbf{\Lambda_N} = diag\{\lambda_{m+1} \geq \lambda_{m+2} \geq ... \geq \lambda_n\}$ of the noise subspace.

We estimate the noise variance σ_v^2 as the mean value of the ($n - m$) minor eigenvalues:

$$\sigma_v^2 = \frac{1}{n-m}\sum_{i=m+1}^{n}\lambda_i \tag{A3}$$

and define the 'robust' whitening matrix as

$$\mathbf{Q}^r = \hat{\mathbf{\Lambda}}_{\mathbf{S}}^{-1/2}\mathbf{V_S^T} = \left(\mathbf{\Lambda_S} - \sigma_v^2\mathbf{I_m}\right)^{-\mathbf{1/2}}\mathbf{V_S^T} \tag{A4}$$

The m-dimensional robust-whitened data vector (zero-mean, unit variance and uncorrelated) can then be expressed as:

$$\tilde{\mathbf{x}} = \hat{\mathbf{\Lambda}}_{\mathbf{S}}^{-1/2}\mathbf{V_S^T}\mathbf{x} = \mathbf{Q}^r\mathbf{x} \tag{A5}$$

where $\mathbf{R}_{\tilde{x}\tilde{x}} \cong \mathbf{I}_m$.

Appendix B. CIISS algorithm

After the robust pre-whitening based on the Signal Subspace criterion 'SS,' in the blind source-extraction procedure 'CII' we firstly identify the mixture unknown matrix A using the following iteration:

$$\hat{\mathbf{A}}(t+1) = \hat{\mathbf{A}}(t) + \mu(t)\left(\mathbf{C}_{x,y}^{1,3}\mathbf{S}_y^3 - \hat{\mathbf{A}}(t)\right) \tag{B1}$$

where $\hat{\mathbf{A}}(t)$ is the estimation of the mixing matrix $\mathbf{A}$ at step t; $\mu(t)$ is the learning-rate parameter; $\mathbf{C}_{x,y}^{1,3} = \mathbf{M}_{x,y}^{1,3} - 3\mathbf{M}_{x,y}^{0,2}\mathbf{M}_{x,y}^{1,1}$ is the 4th-order cross-cumulant matrix computed using sample moment matrices:

$$M_{x,y}^{k,l} = E\left\{\underbrace{x \times ... \times x}_{k}\left(\underbrace{y \times ... \times y}_{l}\right)^T\right\}$$

and $\mathbf{S}_y^3$ is the diagonal matrix of cumulant signs

$$\left[S_y^3\right]_{ii} = sign\left(\left[\mathbf{C}_{x,y}^{1,3}\right]_{ii}\right)$$

Then we compute a separation matrix $\mathbf{W}$ as the pseudo-inverse of $\mathbf{A}$, iterating the process until a fixed measure of convergence is satisfied (Cruces-Alvarez et al., 2000, 2002).

References

Belouchrani A, Cichocki A. A robust whitening procedure in blind source separation context. Electronic Lett 2000;36:2050–1.

Cao J, Murata N, Amari S, Cichocki A, Takeda T, Endo H, Harada N. Single-trial magnetoencephalographic data decomposition and localization based on independent component analysis approach. IEICE Trans Fundam Electronics Commun Comput Sci 2000;9:1757–66.

Choi S, Cichocki A. Blind separation of nonstationary sources in noisy mixtures. Electronic Lett 2000;36:848–9.

Cichocki A, Amari S. Adaptive blind signal and image processing. New York: Wiley; 2002.

Cruces-Alvarez S, Cichocki A, Castedo-Ribas L. An iterative inversion approach to blind source separation. IEEE Trans Neural Networks 2000;11:1423–37.

Cruces-Alvarez S, Castedo-Ribas L, Cichocki A. Robust blind source separation algorithms using cumulants. Neurocomputing 2002;49: 87–118.

Del Gratta C, Pizzella V, Tecchio F, Romani G-L. Magnetoencephalography – a non-invasive brain imaging method with 1 ms time resolution. Rep Prog Phys 2001;64:1759–814.

Delorme A, Makeig S. EEGLAB: an open source toolbox for analysis of single-trial EEG dynamics including independent component analysis. J Neurosci Methods 2003;in press.

Delorme A, Makeig S, Sejnowski T. Automatic artifact rejection for EEG data using high-order statistics and independent component analysis. Proceedings of the 3rd International Workshop on ICA, San Diego, December. 2001. p. 457–62.

Gastaut H. Etude électrocorticographique de la réactivité des rhythmes rolandiques. Rev Neurol 1952;87:176–82.

Gorodnitsky IF, Belouchrani A. Joint cumulant and correlation based signal separation with application to EEG data analysis. Proceedings of the 3rd International Workshop on ICA, San Diego, December. 2001. p. 475–80.

Hari R, Salmelin R. Human cortical oscillations: a neuromagnetic view through the skull. Trends Neurosci 1997;20:44–9.

Hyvärinen A. Gaussian moments for noisy independent component analysis. IEEE Signal Process Lett 1999;6(6):145–7.

Hyvärinen A, Karhunen J, Oja E. Independent component analysis. New York: Wiley; 2001.

Ikeda S, Toyama K. Independent component analysis for noisy data – MEG data analysis. Neural Networks 2000;13(10):1063–74.

Jung TP, Makeig S, Westerfield M, Townsend J, Courchesne E, Sejnowski TJ. Removal of eye activity artifacts from visual event-related potentials in normal and clinical subjects. Clin Neurophysiol 2000; 111:1745–58.

Makeig S, Bell AJ, Jung TP, Sejnowski TJ. Independent component analysis of electroencephalographic data. In: Jordan MI, Kearns MJ, Solla SA, editors. Advances in neural information processing systems, vol. 8. Cambridge, MA: MIT Press; 1996. p. 145–51.

Okada YC, Salenius S. Roles of attention, memory and motor preparation in modulating brain activity in a spatial working memory task. Cereb Cortex 1998;8:80–96.

Tecchio F, Rossini PM, Pizzella V, Cassetta E, Romani G-L. Spatial properties and interhemispheric differences of the sensory hand cortical representation: a neuromagnetic study. Brain Res 1997;767:100–8.

Lee T-W. Independent component analysis: theory and applications. Dordrecht: Kluwer; 1998.

Vigario R, Jousmaki V, Hamalainen M, Hari R, Oja E. Independent component analysis for identification of artifacts in magnetoencephalographic recordings. In: Jordan MI, Kearns MJ, Solla SA, editors. Advances in neural information processing systems, vol. 10. Cambridge, MA: MIT Press; 1997. p. 229–35.

Vorobyov S, Cichocki A. Blind noise reduction for multisensory signals using ICA and subspace filtering, with application to EEG analysis. Biol Cybernet 2002;86:293–303.

Zappasodi F, Tecchio F, Pizzella V, Cassetta E, Romano G-V, Filligoi G, Rossini PM. Detection of fetal auditory evoked responses by means of magnetoencephalography. Brain Res 2001;917:167–73.

Ziehe A, Nolte G, Sander T, Muller KR, Curio G. Artifact reduction in magnetoneurography based on time-delayed second-order correlations. IEEE Trans Biomed Eng 2000;47(1):75–87.

Ziehe A, Nolte G, Sander T, Muller KR, Curio G. A comparison of ICA-based artifact reduction methods for MEG. Proceedings of the 12th International Conference on Biomagnetism. Espoo: Helsinki University of Technolology; 2001. p. 895–8.